

Characterization and optimization of AlGaN/GaN metal-insulator semiconductor heterostructure field effect transistors using supercritical CO_2/H_2O technology

Meihua Liu(刘美华), Zhangwei Huang(黄樟伟), Kuan-Chang Chang(张冠张), Xinnan Lin(林信南), Lei Li(李蕾), and Yufeng Jin(金玉丰)

Citation: Chin. Phys. B, 2020, 29 (**12**): 127101. DOI: 10.1088/1674-1056/abb2

Journal homepage: http://cpb.iphy.ac.cn; http://iopscience.iop.org/cpb

What follows is a list of articles you may be interested in

In-situ SiN combined with etch-stop barrier structure for high-frequency AlGaN/GaN HEMT

Min-Han Mi(宓珉瀚), Sheng Wu(武盛), Ling Yang(杨凌), Yun-Long He(何云龙), Bin Hou(侯斌), Meng Zhang(张濛), Li-Xin Guo(郭立新), Xiao-Hua Ma(马晓华), Yue Hao(郝跃)

Chin. Phys. B, 2020, 29 (**4**): 047104. DOI: 10.1088/1674-1056/ab7746

Mechanism of free electron concentration saturation phenomenon in Te-GaSb single crystal

Ding Yu(余丁), Guiying Shen(沈桂英), Hui Xie(谢辉), Jingming Liu(刘京明), Jing Sun(孙静), Youwen Zhao(赵有文)

Chin. Phys. B, 2019, 28 (**5**): 057102. DOI: 10.1088/1674-1056/28/5/057102

Visualizing light-to-electricity conversion process in InGaN/GaN multi-quantum wells with a p-n junction

Yangfeng Li(李阳锋), Yang Jiang(江洋), Junhui Die(迭俊珲), Caiwei Wang(王彩玮), Shen Yan(严珅), Haiyan Wu(吴海燕), Ziguang Ma(马紫光), Lu Wang(王禄), Haiqiang Jia(贾海强), Wenxin Wang(王文新), Hong Chen(陈弘)

Chin. Phys. B, 2018, 27 (**9**): 097104. DOI: 10.1088/1674-1056/27/9/097104

Intersubband optical absorption of electrons in double parabolic quantum wells of $Al_xGa_{1-x}As/Al_yGa_{1-y}As$

Shu-Fang Ma(马淑芳), Yuan Qu(屈媛), Shi-Liang Ban(班士良)

Chin. Phys. B, 2018, 27 (**2**): 027103. DOI: 10.1088/1674-1056/27/2/027103

Parasitic source resistance at different temperatures for AlGaN/AlN/GaN heterostructure field-effect transistors

Yan Liu(刘艳), Zhao-Jun Lin(林兆军), Yuan-Jie Lv(吕元杰), Peng Cui(崔鹏), Chen Fu(付晨), Ruilong Han(韩瑞龙), Yu Huo(霍宇), Ming Yang(杨铭)

Chin. Phys. B, 2017, 26 (**9**): 097104. DOI: 10.1088/1674-1056/26/9/097104

Characterization and optimization of AlGaN/GaN metal-insulator semiconductor heterostructure field effect transistors using supercritical CO_2/H_2O technology*

Meihua Liu(刘美华), Zhangwei Huang(黄樟伟), Kuan-Chang Chang(张冠张), Xinnan Lin(林信南), Lei Li(李蕾), and Yufeng Jin(金玉丰)†

School of Electronic and Computer Engineering, Peking University Shenzhen Graduate School, Shenzhen 518055, *China*

(Received 8 May 2020; revised manuscript received 31 July 2020; accepted manuscript online 25 August 2020)

The impact of supercritical CO_2/H_2O technology on the threshold-voltage instability of AlGaN/GaN metal-insulator semiconductor high-electron-mobility transistors (MIS-HEMTs) is investigated. The MIS-HEMTs were placed in a supercritical fluid system chamber at 150 °C for 3 h. The chamber was injected with CO_2 and H_2O at pressure of 3000 psi (1 psi ≈ 6.895 kPa). Supercritical H_2O fluid has the characteristics of liquid H_2O and gaseous H_2O at the same time, that is, high penetration and high solubility. In addition, OH^- produced by ionization of H_2O can fill the nitrogen vacancy near the Si_3N_4/GaN/AlGaN interface caused by high temperature process. After supercritical CO_2/H_2O treatment, the threshold voltage shift is reduced from 1 V to 0.3 V. The result shows that the threshold voltage shift of MIS-HEMTs could be suppressed by supercritical CO_2/H_2O treatment.

Keywords: MIS-HEMTs, threshold-voltage instability, gate stress, temperature influence

PACS: 71.55.Eq, 73.20.–r, 73.50.–h **DOI:** 10.1088/1674-1056/abb22f

1. Introduction

GaN and its related material high-electron-mobility transistors (HEMTs) are being intensively studied in power electronics and radio-frequency applications, owing to their attractive superiorities of high breakdown electric field and high saturation electron velocity.[1–3] The high-mobility two-dimensional electron gas (2DEG) generated at the AlGaN/GaN interface enables us to realize power switching transistors having an extremely low on-state resistance, which are applicable to next-generation power conversion systems. Low density electronic states at the AlGaN/GaN interface are necessary because the interface states may cause various operational stability and reliability issues in AlGaN/GaN MIS-HEMTs, such as threshold-voltage instability and current collapse phenomena.[4] To address these issues, it is essential to investigate not only the densities of the electronic states at the AlGaN/GaN interface but also various process conditions to control them.

Supercritical technology can effectively bring elements into materials through supercritical CO_2 fluid, to reduce the trap density and to improve the reliability of devices. Electrical and physical properties of various dielectric layers improved by the low temperature supercritical fluid process have been investigated and demonstrated.[5] Material defects of dielectric can be passivated by supercritical fluid process because of their efficient penetration and damage-free diffusion ability in the microstructures of dielectric layers.[6] Supercritical technology has been applied in the fields of memories and light emitting diodes.[5,7] However, there is no research on effectiveness of GaN power devices, to our best knowledge.

In this work, supercritical CO_2/H_2O technology is proposed to improve the threshold-voltage instability of MIS-HEMTs. After supercritical CO_2/H_2O treatment, improved threshold-voltage instability under gate bias stress and temperature stress is observed. In addition, the AlGaN/GaN heterointerface shows lower trap density (D_{it}) gate leakage current and interface traps are reduced.

2. Fabrication

We describe here in detail the method of fabrication, as well as measurements and characterization of the AlGaN/GaN MIS-HEMTs realized via supercritical CO_2/H_2O technology.

An AlGaN/GaN heterostructure was grown by the metal organic chemical vapor deposition (MOCVD) on a 150 mm Si (111) substrate, which consists of a 4-μm C-doped GaN buffer layer, a 300-nm unintentionally doped GaN channel layer, a 25-nm $Al_{0.25}Ga_{0.75}N$ barrier layer, and a 3-nm GaN cap layer for improving surface morphology. On-wafer Hall measurement yields a sheet resistance of 363 Ω/square, a 2DEG density of 1.1×10^{13} cm^{-2}, and an electron mobility of 1547 $cm^2/V{\cdot}s$. The reported devices were fabricated in a 6-inch silicon foundry.

The process started with the mesa etching, followed by the standard cleaning and deposition of a 30-nm thick Si_3N_4

*Project supported by Shenzhen Science and Technology Innovation Committee (Grant Nos. ZDSYS201802061805105, JCYJ20190808155007550, QJSCX20170728102129176, and JCYJ20170810163407761) and the National Natural Science Foundation of China (Grant No. U1613215).

†Corresponding author. E-mail: yfjin@pku.edu.cn

© 2020 Chinese Physical Society and IOP Publishing Ltd

layer on the heterostructure using low pressure chemical vapor deposition (LPCVD). Standard cleaning was carried out using SC1($H_2O+H_2O_2+NH_4OH$) for 10 min, then deionized water for 10 min, SC2($H_2O+H_2O_2+HCl$) for another 10 min, and finally deionized water for 10 min. The Si_3N_4 layer acted simultaneously as the early surface passivation layer[1] and the gate insulator. Then, a 500-nm SiO_2 passivation layer was deposited by plasma enhanced chemical vapor deposition (PECVD). Ti/Al/Ti/TiN based ohmic contact was formed after recessing the SiO_2 passivation layer and the Si_3N_4 layer. Then, the gate was defined by a combination of SF_6 low power inductively coupled plasma (ICP) etching and buffer oxide etching (BOE). The SiO_2 was first etched down to a thickness of 50 nm by SF_6 plasma, and then fully removed by BOE solution. The remaining thickness of SiO_2 after ICP etching was controlled to be within a deviation of $\pm 10\%$. The BOE would automatically stop at the surface of LPCVD-grown Si_3N_4 due to the extremely high etching selectivity of BOE between PECVD-grown SiO_2 and LPCVD-grown Si_3N_4. Finally, the TiN/Ti/Al gate metal was deposited by physical vapor deposition (PVD) and patterned by dry etching.

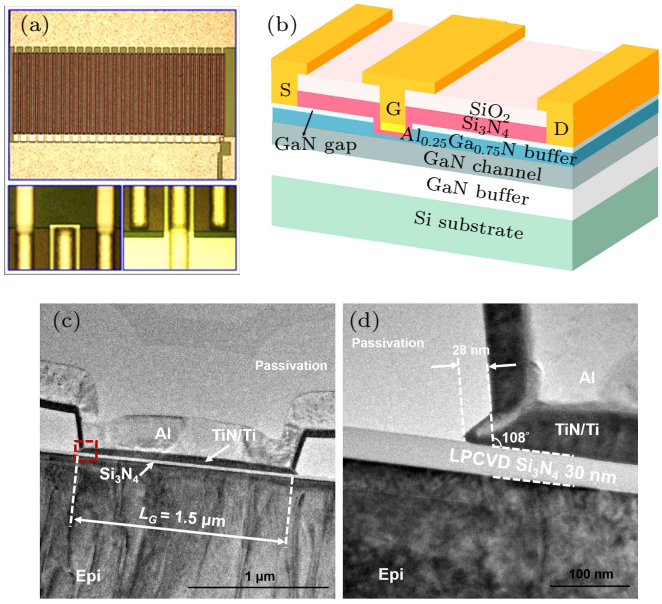


Fig. 1. Schematic overview of the Si_3N_4/GaN/AlGaN/GaN MIS-HEMTs. (a) Overlook schematic of AlGaN/GaN MIS-HEMTs. (b) Cross-section schematic of AlGaN/GaN MIS-HEMTs. (c) Cross-sectional TEM image of the fabricated MIS-HEMTs.[8] (d) Enlarged image of the gate edge.[8]

The source and drain contact areas were recess etched by Cl_2/BCl_3, SF_6, and Cl_2/BCl_3 plasma chronologically, followed by HCl clean treatment and metallization using a gold-free metal scheme. The sources, drains and gates metals were patterned by Cl_2/BCl_3 plasma etching with the one mask. Ohmic contacts were formed by rapid thermal annealing at 850 °C for 45 s in a nitrogen atmosphere. Finally, the devices were passivated by PECVD-grown 585 nm $SiO_2/Si_3N_4/SiO_2$ stacks[9] and connected to the pad metal though vias etched by CHF_3-based plasma. Then, the MIS-HEMTs were put into the chamber of the supercritical fluid system at 150 °C for 3 h, the chamber was injected with CO_2 and H_2O at pressure of 3000 psi.

Figures 1(a) and 1(b) show the cross-section schematic of Si_3N_4/GaN/AlGaN/GaN MIS-HEMTs in this work. The devices under test features a dimension of $L_G/L_{GS}/L_{GD}/W = 1.5/5/10/13050$ μm. Figures 1(c) and 1(d) show the cross-sectional TEM image of the gate structure and the enlarged image of the gate edge.[8] Figure 2 shows that the threshold voltage (V_{th}) of the fresh device is about −8 V and the output saturation current is 430 mA/mm at a gate bias of 0 V.

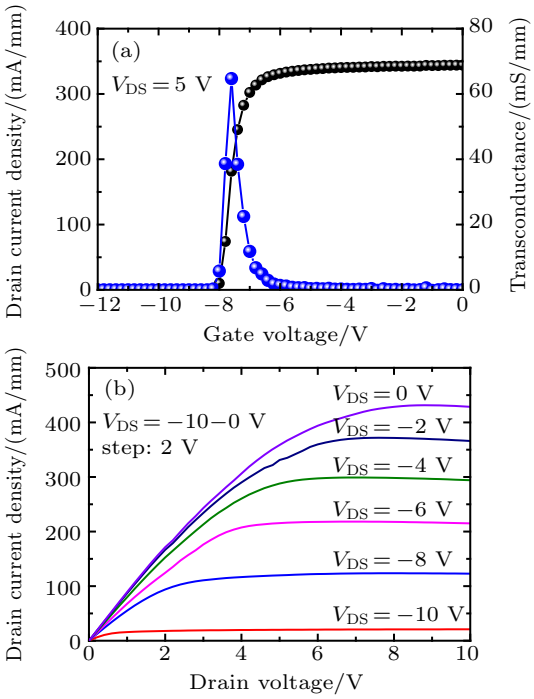


Fig. 2. (a) DC transfer characteristics and (b) output characteristics of the AlGaN/GaN MIS-HEMTs.

3. Results and discussion

3.1. Transport measurements

All our electrical transport measurements were carried out in an Agilent B1500 semiconductor parameter analyzer and an automated Keithley SCS 4200 system.

Due to the high growth temperature in LPCVD, the very surface of the GaN cap layer and the interface (N vacancy) of Si_3N_4/GaN/AlGaN may be relatively defective, which could lead to the trap-induced V_{th} hysteresis phenomena in MIS-HEMTs.[10,11] Conventional static I_D–V_G transfer characteristics were measured at $V_D = 0.5$ V as shown in Fig. 3. All the curves were swept in double mode, with V_G starting from −10 V to −2 V, and then reversed. For the MIS-HEMTs before treatment, significant threshold voltage hysteresis was observed during the forward sweep, suggesting severe trap-

induced drift phenomena. In contrast, the double-mode transfer curves for the MIS-HEMTs after treatment exhibited little threshold voltage hysteresis, indicating the suppression of trap-induced drift phenomena. Furthermore, the on-current of the MIS-HEMTs after treatment is higher than that before treatment, indicating the decrease of positive charge at Si_3N_4/GaN/AlGaN caused by nitrogen vacancy. Physically, because of positive charges present at gate oxide bulk and interface, the magnitude of electric field in the quantum-well increases with decrease in positive charges,[12,13] which leads to the increase of the on current.

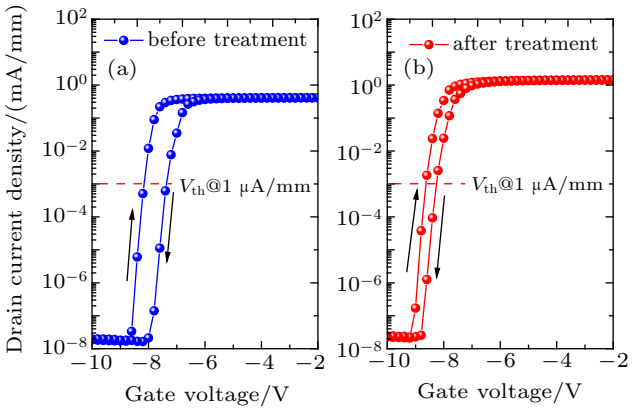


Fig. 3. DC transfer characteristics of the MIS-HEMTs before (a) and after (b) supercritical CO_2/H_2O treatment.

3.2. Threshold voltage stability

It has been reported that state of the art MIS-HMETs still suffers from threshold voltage hysteresis effects induced by forward and reverse gate biases, or temperature increase[14–17] influencing the stability and reliability of these devices in operation. To access threshold voltage stability in the MIS-HEMTs, both the gate stress and the thermal stimulation are applied to the devices, and the change in threshold voltage was monitored.

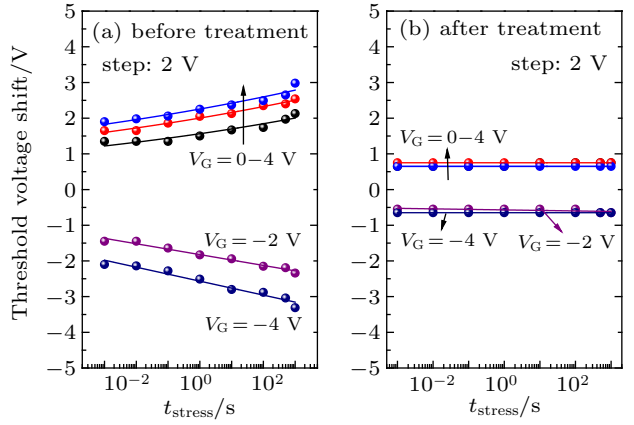


Fig. 4. Stress sequence of AlGaN/GaN MIS-HEMTs before (a) and after (b) supercritical CO_2/H_2O treatment.

For the gate stress measurement, the stress is applied only to the gate terminal at room temperature with $V_D = 0.5$ V. A stress of $V_G = -4$, -2, 0, 2 and 4 V was used to evaluate the bias induced threshold voltage instability. The total stress time was fixed at 1000 s. V_{th} hysteresis was monitored by fast I_D–V_G measurement after certain stress time intervals. V_{th} is determined at an I_D of 1 μA/mm. A clear dependence on the gate bias is observed in Fig. 4. For the AlGaN/GaN MIS-HEMTs before supercritical CO_2/H_2O treatment, threshold voltage hysteresis was measured under different stress voltages from 1.35 V to 3.31 V. In contrast, for AlGaN/GaN MIS-HEMTs after treatment, threshold voltage hysteresis was measured from 0.55 V to 0.75 V. The result indicates that the trapping of interface states is improved after supercritical CO_2/H_2O treatment.

The temperature dependent V_{th} hysteresis is evaluated by submitting the MIS-HEMTs to thermal stimulation from room 310 K to 390 K with a 10 K step at $V_D = 5$ V. Figure 5 shows the transfer characteristics at various temperatures. Before treatment, when the temperature rises from 310 K to 390 K, the threshold voltage hysteresis by 0.22 V. After treatment, when the temperature rises from 310 K to 390 K, the threshold voltage hysteresis by 0.1 V. Compared with that before treatment, the threshold voltage decreases by 0.12 V, which indicates that the threshold voltage is less affected by temperature and the interface defects are induced.

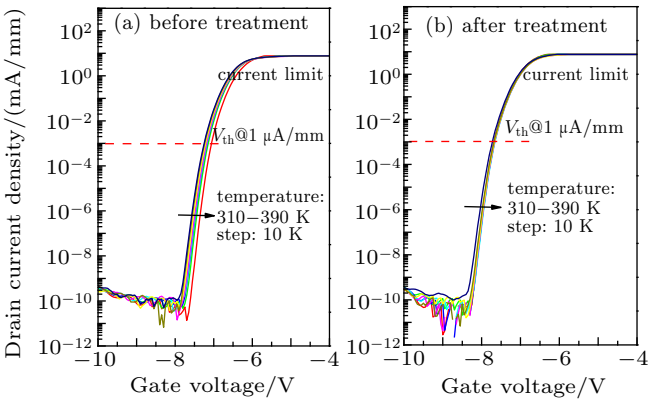


Fig. 5. Temperature-dependent transfer characteristics of the AlGaN/GaN MIS-HEMTs before (a) and after (b) supercritical CO_2/H_2O treatment.

3.3. AlGaN/GaN interface trap characterization

Double-mode gate capacitance–voltage (C–V) measurements from -10 V to -4 V was also conducted on the devices with shorted source and drain at a frequency of 10 kHz. As shown in Fig. 6, before treatment, hysteresis of MIS-HEMTs is about 1 V. After treatment, hysteresis of MIS-HEMTs is about 0.3 V, which is reduced by 0.7 V. Furthermore, a steeper C–V curve for the MIS-HEMTs after treatment can be observed, indicating that the gate dielectric/barrier layer interface has low interface trap density.[18]

The G_P can be expressed as

$$\frac{G_P}{\omega} = \frac{qD_{it}}{2\omega\tau_{it}} \ln[1 + (\omega\tau_{it})^2], \tag{1}$$

where ω is the radial frequency and τ_{it} is the trap time constant given by the Shockley–Read–Hall statistics.[19]

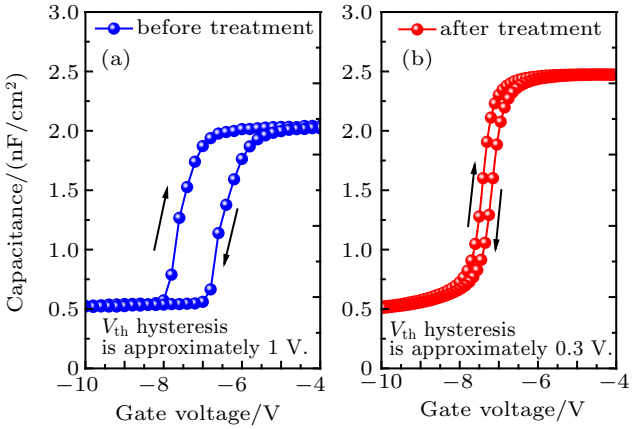


Fig. 6. Capacitance measurements for the AlGaN/GaN MIS-HEMTs before (a) and after (b) supercritical CO_2/H_2O treatment.

Figure 7 shows the behavior of G_P/ω versus ω measured at selected gate biases for the MIS-HEMTs before and after supercritical CO_2/H_2O treatment biased at selected gate voltage. Interface trap density was extracted by fitting the experimental data.

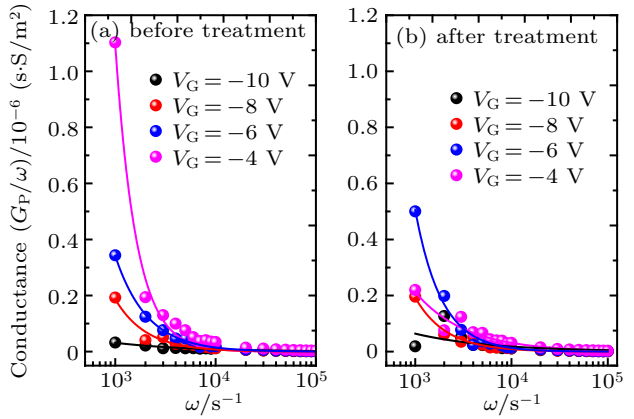


Fig. 7. Frequency-dependent conductance as a function of radial frequency for the MIS-HEMTs before (a) and after (b) supercritical CO_2/H_2O treatment biased at selected gate voltage.

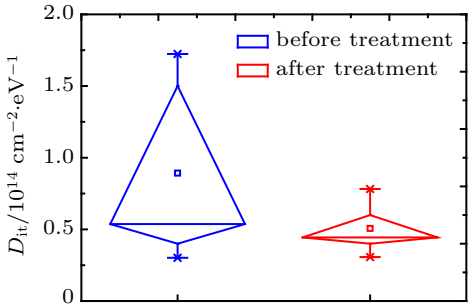


Fig. 8. AlGaN/GaN interface trap density extracted through frequency-dependent conductance for the MIS-HEMTs before and after supercritical CO_2/H_2O treatment.

Trap density extracted through frequency-dependent conductance as a function of radio frequency for the MIS-HEMTs before and after supercritical CO_2/H_2O treatment are plotted in Fig. 8. For the AlGaN/GaN MIS-HEMTs before supercritical CO_2/H_2O treatment, the trap density at the AlGaN/GaN heterointerface ranges from 3×10^{13} to 1.7×10^{14} cm^{-2}·eV^{-1}. For the AlGaN/GaN MIS-HEMTs after supercritical CO_2/H_2O treatment, the trap density at the AlGaN/GaN heterointerface ranges from 4×10^{13} to 6×10^{13} cm^{-2}·eV^{-1}. In addition, trap density was induced by twice after supercritical CO_2/H_2O treatment.

3.4. Si_3N_4/GaN/AlGaN interface trap characterization

Figure 9 shows Ga 3d (left) and Si 2p (right) core-level spectra at the Si_3N_4/GaN cap interface in the 8-nm Si_3N_4/GaN/AlGaN sample. After supercritical CO_2/H_2O treatment, the proportion of Ga–O bonds increases from 0.03% to 16.32%. The proportion of Si–N bonds decreases from 99.83% to 83.64%. At the same time, the proportion of Ga dangling bonds decreases from 0.14% to 0.04%. The proportion of Si dangling bonds decreases from 3.41% to 1.33%. The change of the proportion of chemical bonds indicates that part of the N vacancies is filled after supercritical CO_2/H_2O treatment.

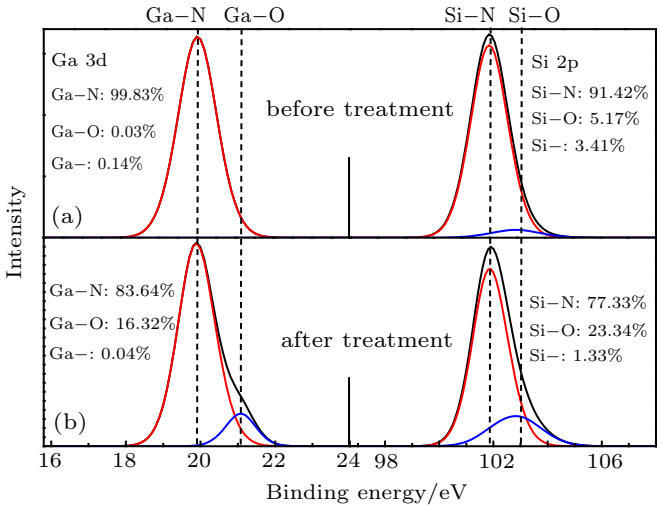


Fig. 9. Ga 3d (left) and Si 2p (right) core-level spectra at the Si_3N_4/GaN cap interface in the 8-nm-Si_3N_4/GaN/AlGaN/GaN samples (a) before supercritical CO_2/H_2O treatment and (b) after supercritical CO_2 treatment. Each measured spectrum (symbol) is resolved into two Gaussian functions that correspond to M in M-(solid magenta line) and M-(solid blue line) bonds. M represents Ga (left) or Si (right). The solid blue magenta line is a superposition of the two fitting functions.

3.5. Supercritical CO_2 technology mode

Figure 10 shows the supercritical CO_2/H_2O technology model of AlGaN/GaN MIS-HEMTs. The MIS-HEMTs were put into the chamber of the supercritical fluid system at 150 °C for 3 h, the chamber was injected with CO_2 at the pressure of 3000 psi. CO_2 is a double bond structure with large activation energy and stable chemical properties. It does not participate in the reaction during supercritical CO_2/H_2O treatment. During the process of supercritical CO_2 treatment, H_2O in supercritical system also reaches the supercritical state. Supercritical H_2O fluid has the characteristics of liquid H_2O and gaseous

H_2O at the same time, that is, high penetration and high oxidation, which penetrate into the MIS-HEMTs.

$$H_2O = OH^- + H^+. \tag{2}$$

Lattice mismatching caused the defects of the Si_3N_4/GaN/AlGaN/GaN, leading to the trap-induced drift phenomena of AlGaN/GaN MIS-HEMTs. Owing to the increase of OH bonds, the hydrogen ions generated by broken OH bonds were attracted to gate area when supplied a negative bias, filling in the nitrogen vacancy. With supercritical CO_2/H_2O technology, the defects are fixed by restoring dangling bonds.

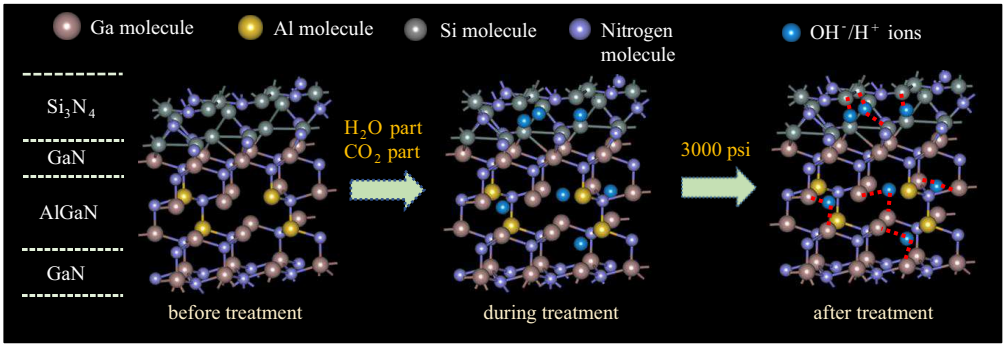


Fig. 10. The supercritical CO_2/H_2O technology model of AlGaN/GaN MIS-HEMTs.

4. Conclusion

In summary, high performance AlGaN/GaN MIS-HEMTs realized via supercritical CO_2/H_2O treatment has been designed, fabricated, and measured. By comparing the devices before and after supercritical CO_2/H_2O treatment, we find that supercritical CO_2/H_2O treatment can effectively improve the quality of Si_3N_4/GaN/AlGaN/GaN interface and suppress the hysteresis of threshold voltage. After supercritical CO_2/H_2O treatment, the optimized Si_3N_4/GaN/AlGaN/GaN MIS-HEMTs demonstrate a 0.7 V threshold voltage hysteresis decrease, and a lower interface trap density decrease of almost 2 times. The results presented in this study indicate that the supercritical CO_2/H_2O technology is effective in reducing the interface states and improving the electrical properties of the AlGaN/GaN MIS-HEMTs.

References

[1] Ikeda N, Niiyama Y, Kambayashi H, Sato Y, Nomura T, Kato S and Yoshida S 2010 *Proc. IEEE* **98** 1151
[2] Liu Z H, Ng G I, Arulkumaran S, Maung Y K T, Teo K L, Foo S C, Sahmuganathan V, Xu T and Lee C H 2010 *IEEE Electron Device Lett.* **31** 96
[3] Chen K J and Zhou C 2011 *Phys. Status Solidi* **208** 434
[4] Zhang Z, Li W, Fu K, Yu G, Zhang X, Zhao Y, Sun S, Song L, Deng X, Xing Z, Yang L, Ji R, Zeng C, Fan Y, Dong Z, Cai Y and Zhang B S 2017 *IEEE Electron Device Lett.* **38** 236
[5] Chattopadhyay P and Gupta R B 2001 *Int. J. Pharm.* **228** 19
[6] Tsai C T, Chang T C, Liu P T, Yang P Y, Kuo Y C, Kin K T, Chang P L and Huang F S 2007 *Appl. Phys. Lett.* **91** 012109
[7] Chang K C, Pan C H, Chang T C, Tsai T M, Zhang R, Lou J C, Young T F, Chen J H, Shih C C, Chu T J, Chen J Y, Su Y T, Jiang J P, Chen K H, Huang H C, Syu Y E, Gan D S and Sze S M 2013 *IEEE Electron Device Lett.* **34** 617
[8] Sun H, Wang M, Chen J, Liu P, Kuang W, Liu M, Hao Y and Chen D 2018 *IEEE Trans. Electron Devices* **65** 11
[9] Zhang K, Kong Y, Zhu G, Zhou J, Yu X, Kong C, Li Z and Chen T 2017 *IEEE Electron Device Lett.* **38** 615
[10] Hashizume T and Hasegawa H 2004 *Appl. Surf. Sci.* **234** 1
[11] Robertson J 2009 *Appl. Phys. Lett.* **94** 152104
[12] Amarnath G, Swain R and Lenka T R 2017 *Int. J. Numerical Modelling: Electronic Networks Devices and Fields* **31** e2268
[13] Swain R, Jena K and Lenka T R 2016 *Mater. Sci. Semiconduct. Process.* **53** 66
[14] Wu T L, Marcon D, Zahid M B, Hove M V, Decoutere S and Groeseneken G 2013 *IEEE International Reliability Physics Symposium* **10** 1109
[15] Meneghini M, Rossetto I, Bisi D, Ruzzarin M, Hove M V, Stoffels S, Wu T L, Marcon D, Decoutere S, Meneghesso G and Zanoni E 2016 *IEEE Electron Device Lett.* **37** 474
[16] Wu T L, Franco J, Marcon D, Jaeger B D, Bakeroot B, Stoffels S, Hove M V, Groeseneken G and Decoutere S 2016 *IEEE Trans. Electron Devices* **63** 1853
[17] Lagger P, Reiner M, Pogany D and Ostermaier C 2014 *IEEE Trans. Electron Devices* **61** 1022
[18] Wang H C, Lumbantoruan F J, Hsieh T E, Wu C H, Lin Y C and Chang E Y 2018 *IEEE J. Electron Devices Soc.* **6** 1136
[19] Stoklas R, Gregušová D, Hasenöhrl S and Brytavskyi E 2018 *Appl. Surf. Sci.* **461** 255